Drop formation in a one-dimensional approximation of the Navier–Stokes equation

By JENS EGGERS[1]† AND TODD F. DUPONT[2]

[1] Department of Mathematics and the James Franck Institute, the University of Chicago, 5734 University Avenue, Chicago, IL 60637, USA

[2] Department of Computer Science, the University of Chicago, 1100 East 58th Street, Chicago, IL 60637, USA

We consider the viscous motion of a thin axisymmetric column of fluid with a free surface. A one-dimensional equation of motion for the velocity and the radius is derived from the Navier–Stokes equation. We compare our results with recent experiments on the breakup of a liquid jet and on the bifurcation of a drop suspended from an orifice. The equations form singularities as the fluid neck is pinching off. The nature of the singularities is investigated in detail.

1. Introduction

A problem fundamental to the study of nonlinear partial differential equations is the nature of their singularities. Perhaps the most famous (and unsolved) problem is the suspected blow-up of the derivatives of the velocity field in the three-dimensional Euler equation (Majda 1986). Shocks, i.e. discontinuities in the velocity, are the type of singularity displayed by the one-dimensional inviscid Burgers equation (Smoller 1983).

A different type of singularity has to be expected from three-dimensional free surface flow, which we will consider here. A similar study of a two-dimensional flow has been conducted recently (Constantin *et al.* 1993). Surface tension will tend to make the surface as small as possible by reducing the radius. The classical stability analysis of an infinite cylinder of fluid by Rayleigh (1878) shows that the radius does not decrease uniformly: owing to the constraint of mass conservation the fastest growing mode is the one with wavelength $\lambda \approx 9r_0$, where r_0 is the radius of the cylinder. Consequently, the fluid cylinder will decay into drops of roughly that size.

Once the radius becomes zero locally, i.e. the original column of fluid separates, the description in terms of a radius function breaks down. Hence the equations must develop a singularity at that point. Although linear stability analysis gives a reasonable estimate of the size of the droplets formed, it completely fails to predict the shape of the surface once an appreciable deformation of the original cylinder is reached (Chaudhary & Redekopp 1980). For example it does not explain the fact that the cylinder does not break up uniformly. Rather, regular sized drops are, under most circumstances, followed by much smaller 'satellite drops'. Even higher-order perturbation theory (Chaudhary & Redekopp 1980; Chaudhary & Maxworthy 1980) gives only a qualitative prediction of the unequal drop sizes, but is not able to describe the shape of the fluid anywhere close to pinch-off. This is not very surprising, because the characteristic time of the linear instability is close to the time distance from the singularity, where expansions in the radius and the velocity are bound to break down.

† Present address: Universität GH Essen, FB7, 45117 Essen, Germany.

Therefore a complete treatment of the nonlinearities is needed. The full Navier–Stokes equaton with free boundary conditions is extremely complicated, for both analytical and numerical studies. The only simulations of axisymmetric drops we are aware of were restricted to irrotational, inviscid flow (Becker, Hiller & Kowalewski 1991). But even with this restriction simulations close to the singularity become extremely costly, since the neck region requires high resolution. A reduction of the problem to one dimension will give huge savings in computer time, making closeups of the singularity possible.

There already exist some one-dimensional equations for axisymmetric free surface flow (Lee 1974; Bogy 1979). Lee only considers the inviscid case. Bogy's equations allow for dissipation but are very complicated in structure and do not have a clear connection with the original Navier–Stokes equation. We will therefore derive a set of one-dimensional equations by expanding the radial variable in a Taylor series and keeping only the lowest-order terms of the Navier–Stokes equation. Several invariances and conservation laws of the Navier–Stokes equation are preserved. This will be the subject of the second section, along with a linear stability analysis.

Integrating the equations near the singularity proves to be very difficult, since the problem becomes very stiff due to the large range of lengthscales. We develop a fully implicit centred difference method. This scheme is then modified to treat the convection term $v v_z$ by an upwinding technique which ensures negative definiteness of the numerical dissipation. The numerical scheme is detailed in §3.

There is a fair amount of work applying one-dimensional equations to the breakup of jets (Lee 1974; Bogy 1979), liquid bridges (Meseguer 1983) or hanging drops (Cram 1984). There is also work in this spirit on films lining a cylindrical tube (Johnson *et al.* 1991). Yet a detailed comparison between experiments and one-dimensional models within the nonlinear regime is missing. Therefore, we try to compare experimental drop profiles with simulations close to the breakup point. This is found in §4 for two recent experiments.

The first experiment (Chaudhary & Maxworthy 1980) examines the decay of a free jet of water, the second observes how a hanging drop detaches after it is adiabatically filled out of an orifice (Peregrine, Shoker & Symon 1990). We also produce an example with a high-viscosity fluid. Simulations and experiments agree very well, giving ample support to the idea that droplet breakup can be well described by one-dimensional equations.

In the next section we take a closer look at the pinch region. We discuss a similarity theory for the non-viscous case and explain its failure. All viscous solutions are determined by universal scaling functions close to the pinch point. The concluding section briefly discusses the approximation used in relation to other types of approximations, its higher-order versions, and the full Navier–Stokes or Euler equations. Finally, we indicate directions of future research.

2. The equations of motion

We start from the Navier–Stokes equation for an axisymmetric column of fluid with kinematic viscosity ν, density ρ, and surface tension γ. In cylindrical coordinates it reads (Landau & Lifshitz 1984)

$$\partial_t v_r + v_r \partial_r v_r + v_z \partial_z v_r = -\partial_r p/\rho + \nu(\partial_r^2 v_r + \partial_z^2 v_r + \partial_r v_r/r - v_r/r^2), \tag{1}$$

$$\partial_t v_z + v_r \partial_r v_z + v_z \partial_z v_z = -\partial_z p/\rho + \nu(\partial_r^2 v_z + \partial_z^2 v_z + \partial_r v_z/r) - g, \tag{2}$$

where v_z is the velocity along the axis, v_r the velocity in the radial direction, and p the

pressure. The acceleration due to gravity g points in the negative z-direction. The continuity equation reads

$$\partial_r v_r + \partial_z v_z + v_r/r = 0. \tag{3}$$

Equations (2) and (3) hold for $0 \leqslant r < h(z, t)$. The balance of normal force gives

$$\boldsymbol{n} \cdot \boldsymbol{\sigma} \cdot \boldsymbol{n} = -\gamma(1/R_1 + 1/R_2), \tag{4}$$

where $\boldsymbol{\sigma}$ is the stress tensor, $\boldsymbol{n}$ is the outward normal, and R_1 and R_2 are the principal radii of curvature. The tangential force balance is

$$\boldsymbol{n} \cdot \boldsymbol{\sigma} \cdot \boldsymbol{t} = 0. \tag{5}$$

Explicitly, this gives

$$\frac{p}{\rho} - \frac{2\nu}{1+h'^2}[\partial_r v_r + (\partial_z v_z)h'^2 - (\partial_r v_z + \partial_z v_r)h'] = \frac{\gamma}{\rho}\left(\frac{1}{R_1} + \frac{1}{R_2}\right)\Big|_{r=h} \tag{6}$$

for the normal forces, and

$$\frac{\nu}{1+h'^2}[2(\partial_r v_r)h' + (\partial_r v_z + \partial_z v_r)(1-h'^2) - 2(\partial_z v_z)h'] = 0\,|_{r=h} \tag{7}$$

for the tangential forces. The prime refers to differentiation with respect to z. Finally, the surface has to move with the velocity field at the boundary:

$$\partial_t h + v_z h' = v_r|_{r=h}. \tag{8}$$

Since we are going to look at thin columns of fluid relative to their elongation, we expand in a Taylor series with respect to r. By symmetry we get

$$v_z(z, r) = v_0 + v_2 r^2 + \dots, \tag{9}$$

and (3) is satisfied by choosing v_r to be

$$v_r(z, r) = -\tfrac{1}{2}v_0' r - \tfrac{1}{4}v_2' r^3 - \dots. \tag{10}$$

The pressure is expanded in the same way:

$$p(z, r) = p_0 + p_2 r^2 + \dots. \tag{11}$$

We now insert (9)–(11) into (1), (2), and (6)–(8) and solve the equations to lowest order in r. In the case of (2) this gives

$$\partial_t v_0 + v_0 v_0' = -p_0'/\rho + \nu(4v_2 + v_0'') - g. \tag{12}$$

Equation (1) is identically satisfied to lowest order.

Remembering that h' is also of order r we get from (6) an expression for the pressure p_0 in (12):

$$p_0/\rho + \nu v_0' = (\gamma/\rho)(1/R_1 + 1/R_2). \tag{13}$$

Similarly, (7) gives an expression involving v_2:

$$-v_0' h' + 2v_2 h - \tfrac{1}{2}v_0'' h - 2v_0' h' = 0. \tag{14}$$

Equations (13) and (14) can be used to eliminate p_0 and v_2 from (12) giving

$$\partial_t v_0 = -v_0 v_0' - \frac{\gamma}{\rho}\left(\frac{1}{R_1} + \frac{1}{R_2}\right)' + 3\nu\frac{(h^2 v_0')'}{h^2} - g. \tag{15}$$

The surface condition (8) gives to lowest order

$$\partial_t h = -v_0 h' - \tfrac{1}{2} v_0' h. \tag{16}$$

The formula for the mean curvature $\tfrac{1}{2}(1/R_1 + 1/R_2)$ of a body of revolution is known from differential geometry (do Carmo 1976). Thus, dropping the index on v_0 and denoting the surface tension contribution of the pressure by p, we finally get

$$\partial_t v = -vv_z - p_z/\rho + 3\nu(h^2 v_z)_z/h^2 - g, \tag{17}$$

$$p = \gamma \left[\frac{1}{h(1+h_z^2)^{\frac{1}{2}}} - \frac{h_{zz}}{(1+h_z^2)^{\frac{3}{2}}} \right]$$

and

$$\partial_t h = -vh_z - \tfrac{1}{2} v_z h. \tag{18}$$

Here the index z refers to differentiation with respect to z. When solving the set of equations (17), (18) for $z \in [-l, l]$ we impose the boundary conditions

$$h(\pm l, t) = h_\pm \tag{19}$$

and

$$v(\pm l, t) = v_\pm. \tag{20}$$

The set of equations (17)–(20) will concern us for the rest of this paper. We reiterate that the physical velocity field (9), (10) described by (17), (18) has both radial and longitudinal components with a non-trivial r-dependence. The physical pressure (11) also carries contributions from the shear stress. This should be born in mind when we refer to v and p in (17), (18) as 'velocity' and 'pressure'.

There are two important conservation laws for this simplified system. First, mass conservation means

$$\partial_t V = \pi h^2 v \big|_l^{-l}, \tag{21}$$

$$V = \pi \int_{-l}^{l} h^2 \, dz. \tag{22}$$

Second, the sum of the kinetic energy

$$E_{kin} = \tfrac{1}{2} \pi \rho \int_{-l}^{l} h^2 v^2 \, dz \tag{23}$$

and the potential energy

$$E_{pot} = 2\pi\gamma \int_{-l}^{l} h(1+h_z^2)^{\frac{1}{2}} \, dz + \pi\rho g \int_{-l}^{l} h^2 z \, dz \tag{24}$$

obeys the balance equation

$$\partial_t (E_{kin} + E_{pot}) = \mathscr{D} - \pi \left(\tfrac{1}{2}\rho h^2 v^3 - \frac{2\gamma h h_z \partial_t h}{(1+h_z^2)^{\frac{1}{2}}} + ph^2 v - 3\nu\rho v h^2 v_z + \rho g h^2 v z \right) \bigg|_{-l}^{l}. \tag{25}$$

So, apart from boundary terms the total energy changes with the rate of energy dissipation

$$\mathscr{D} = -3\pi\nu\rho \int_{-l}^{l} (hv_z)^2 \, dz. \tag{26}$$

Since $\mathscr{D}$ is negative definite, it follows that, without external driving (boundary terms in (25)), the total energy can only decrease. Note that the potential energy for the full equations is precisely (24), so that the exact surfaces of static equilibrium are also equilibrium surfaces of the model: they are states which minimize E_{pot} (Landau & Lifshitz 1984). Famous examples are the equilibrium shapes of pendant drops (Michael & Williams 1976). This was the reason for keeping lower-order terms in the expression for p: in a consistent expansion by orders of r the expression for p simply would have been

$$p = \gamma(1/h - h_{zz}),$$

resulting in a different form of the potential energy. We also note that $\mathscr{D}$ is *not* negative definite for the viscous term as cited by Cram (1984). His term νv_{zz} may feed energy into the fluid, which we found to prevent the system from reaching an equilibrium state.

Although of limited applicability in practice, it is instructive to repeat the stability analysis for a fluid cylinder in the case of our model. Assume that a cylinder of radius r_0 receives a sinusoidal perturbation of wavelength $\lambda = 2\pi/k$; then

$$r(z, t) = r_0[1 + \varepsilon(t)\cos(kz)],$$

$$v(z, t) = \varepsilon(t)v_0\sin(kz).$$

Assuming $\varepsilon(t) = \varepsilon\exp(\omega t)$, (17) and (18) give to lowest order in ε

$$\omega v_0 = -(\gamma/\rho)(k/r_0 - r_0 k^3) - 3\nu v_0 k^2$$

and

$$\omega = -\tfrac{1}{2}v_0 k,$$

respectively. This leaves us with the dispersion relation

$$\omega^2 = \omega_0^2 \tfrac{1}{2}((r_0 k)^2 - (r_0 k)^4) - 3\nu\omega k^2, \tag{27}$$

$$\omega_0^2 = \gamma/r_0^3\rho.$$

The solution of (27) is

$$\omega = \omega_0\left\{\left[(kr_0)^2\tfrac{1}{2}(1 - (kr_0)^2) + \frac{9}{4}\frac{l_\nu}{r_0}(kr_0)^4\right]^{\frac{1}{2}} - \frac{3}{2}\left(\frac{l_\nu}{r_0}\right)^{\frac{1}{2}}(kr_0)^2\right\}, \tag{28}$$

where

$$l_\nu = \nu^2\rho/\gamma \tag{29}$$

is a viscous lengthscale. Both the limits of zero viscosity,

$$\omega = \omega_0[\tfrac{1}{2}(kr_0)^2(1 - (kr_0)^2)]^{\frac{1}{2}} \tag{30}$$

and high viscosity,

$$\omega = \frac{\gamma}{r_0\rho\nu}\tfrac{1}{6}(1 - (kr_0)^2), \tag{31}$$

coincide with the exact result (Chandrasekhar 1961) if an expansion to lowest order in kr_0 is made.

Equation (28) shows that there is an instability for long wavelengths, the stability boundary being $kr_0 = 1$, independent of ν. In the case of a random disturbance, however, the relevant quantity is the *most unstable* or fastest growing mode. In the general case this is

$$(kr_0)_{max}^2 = \frac{1}{2[1 + (\tfrac{9}{2}l_\nu/r_0)^{\frac{1}{2}}]}. \tag{32}$$

For $\nu = 0$, the most unstable wavelength is therefore $\lambda_{max} = 8.89 r_0$ instead of the exact value of $9.01 r_0$ (Chandrasekhar 1961). In the limit of very high viscosity the infinite-wavelength perturbation becomes the most unstable one.

3. Numerical procedure

The numerical approximations were computed using a rather simple finite difference scheme. The spatial mesh is a highly non-uniform, graded mesh; its refinement is based on the behaviour of the computed solution. The time-integration method is an adaptive fully implicit θ-weighted scheme.

Let the space mesh be

$$z_1 < z_2 < \ldots < z_N$$

and adopt the following notation:

$$\Delta z_i = z_{i+1} - z_i,$$

$$z_{i+\frac{1}{2}} = \tfrac{1}{2}(z_i + z_{i+1}),$$

$$\Delta z_{i+\frac{1}{2}} = z_{i+\frac{3}{2}} - z_{i-\frac{1}{2}}.$$

The meshes used were always constrained to satisfy

$$\frac{1}{2} \leqslant \frac{\Delta z_i}{\Delta z_{i+1}} \leqslant 2.$$

The solution at each time level is defined by two arrays, $\{h_i\}_{i=0}^{N}$ and $\{v_i\}_{i=1}^{N-1}$; the quantity h_i is the value of the approximate radius h at the mesh point z_i and the value v_i gives the value of the approximate velocity v at the point $z_{i+\frac{1}{2}}$. In describing the discrete equations for a particular time step it is convenient to let dv_i and dh_i denote the changes in v_i and h_i, respectively, that take place over the step.

Difference analogues of the v-equation, (17), were written corresponding to each point $z_{i+\frac{1}{2}}$ and the difference analogues of the h-equation, (18), were written for each z_i. The time-derivative term was approximated by $dv_i/\Delta t$ or $dh_i/\Delta t$, respectively. The relation for p was used to define it at each point z_i in terms of h at z_{i-1}, z_i, and z_{i+1}, using centred differences for the h_z term and a second difference for h_{zz}. (Near the bottom of a pendant drop this was changed; see the remarks just after (34).) This defines p at each time level in terms of h at that level.

In setting up the difference equations that mimic (17) and (18) the spatial terms (everything except the time-derivative terms) are evaluated using a weighted average of the current value and the yet-to-be-computed value. These 'mid-step' values can be written as $v_i + \theta \, dv_i$ and $h_i + \theta \, dh_i$. With $\theta = 0.5$ this gives a second-order correct in the time-difference equation, but we used θ slightly larger than 0.5 (typically $\theta = 0.55$). Using θ close to one half gives a small first-order truncation term (say 10% of the first-order backward-difference equation). Taking $\theta > 0.5$ gives smoother discrete solutions than $\theta = 0.5$.

The approximation of the vv_z term at $z_{i+\frac{1}{2}}$ is done as follows:

$$vv_z \approx v_i(v_{i+1} - v_{i-1})/\Delta z_{i+\frac{1}{2}} + \text{NVT},$$

where NVT is the numerical viscosity term that 'upwinds' this nonlinear convective term. The NVT is structured so that it is an energy dissipation term of small size; the usual technique of simply skewing the difference equation in the direction that the fluid

is coming from does not assure such a property. The NVT term that we use is a difference analogue of

$$\frac{-1}{h^2}(h^2 \tilde{\nu}(z) \, v_z)_z,$$

where $\tilde{\nu}(z) = \vartheta v \Delta z$ and ϑ is a non-negative parameter. Specifically,

$$\tilde{v}_{i+1} = \frac{\Delta z_i \, v_{i+1} + \Delta z_{i+1} \, v_i}{\Delta z_i + \Delta z_{i+1}},$$

$$h^2 \tilde{\nu}(z) \, v_z |_{i+1} = h_{i+1}^2 (v_{i+1} - v_i) \, \vartheta \tilde{v}_{i+1},$$

$$NVT = \frac{-1}{(\frac{1}{2}(h_{i+1} + h_i))^2} \frac{h^2 \tilde{\nu}(z) \, v_z |_{i+1} - h^2 \tilde{\nu}(z) \, v_z |_i}{\Delta z_i}.$$

The rest of the v-equation formed as central differences. Note that associating p with the z_i gives p_z at the $z_{i+\frac{1}{2}}$ points. The viscosity term in (17) is very similar to the NVT term; the $\tilde{\nu}$-term is just the constant ν.

The h-equation at z_i has two spatial terms. The first, vh_z, is approximated by $\tilde{v}_i(h_{i+1} - h_{i-1})/(\Delta z_i + \Delta z_{i-1})$. The second, $\frac{1}{2}v_z h$, is approximated by

$$\left(\frac{v_i - v_{i-1}}{\Delta z_i + \Delta z_{i-1}} \right) h_i.$$

In solving the nonlinear difference equations we use Newton's method. Many of our simulations used only one Newton step per time step, starting from an initial guess based on linear extrapolation from the previous two time levels. It is quite easy, and reasonably efficient, to control the time step in such a way that one step of Newton's method reduces the error to very close to rounding error. It is worthwhile pointing out that even if the decision is made to only use one step of Newton's method it is useful to code it in general, since observing quadratic convergence of the iteration is a good check on whether the linearization has been done correctly.

4. Comparison with experiment

The first experiment we consider studies the breakup of a liquid jet (Chaudhary & Maxworthy 1980). Water is pumped through a nozzle at high speed to form a liquid column virtually unaffected by gravity. A periodic perturbation, whose amplitude and frequency can be controlled, is applied to the jet as it leaves the nozzle. The system is allowed to reach a steady state, in which the jet at a sufficiently large distance from the nozzle has completely broken up into droplets. Photographs of this stationary configuration are taken.

We try to model the experiment as closely as possible, but since we can only simulate up to the point of the first singularity (owing to limitations of our current program) we cannot reach the stationary state. Instead, we fix $h_+ = h_- \equiv r_0 \ll l$ and $v_+ = v_- \equiv V$, and over a period of eight wavelengths smoothly turn on a small sinusoidal perturbation to v_-.

Thus the parameters of the simulation are the length of the jet $2l$, its initial radius r_0, the fluid parameters γ/ρ and ν, the speed of the jet V, and the amplitude V_p and frequency f_p of the perturbation. We chose $r_0/2l = 0.004$, so the size of the drops is very small compared with the jet length and the precise value of this ratio is immaterial. V_p was adjusted to make breakup times conform with experiment. The remaining
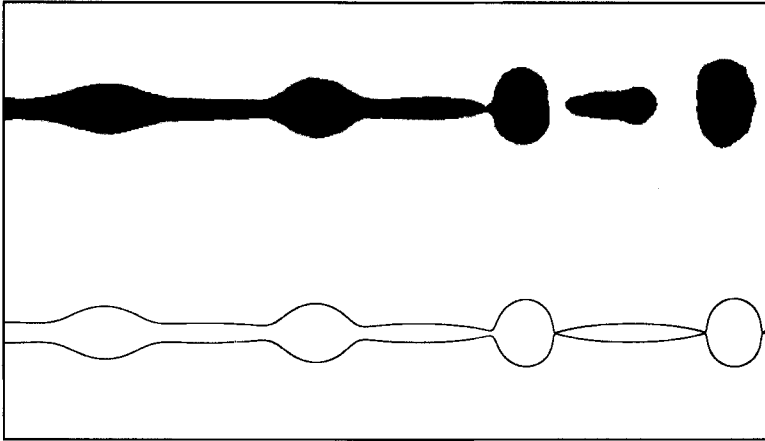
FIGURE 1. Comparison between a decaying water jet (from Chaudhary & Maxworthy 1980) (upper) and our simulation (lower). We processed the original image so as produce a white background. The nozzle is to the left. The point where the first drop detaches from the experimental jet has been aligned with the corresponding point of our simulations. The horizontal scale has been adjusted as well. The parameters are $\lambda/r_0 = 14.57$, $l_\nu/r_0 = 6.54 \times 10^{-4}$, and $\beta^2 = 239$. The fluid parameters in the experiment differ slightly from the ones quoted in table 1, due to additives.

	Water 20 °C	Glycerol 20 °C	Glycerol 25 °C
ν [cm^2 s^{-1}]	1.00×10^{-2}	11.8	7.6
γ/ρ [cm^3 s^{-2}] fluid–air interface	72.9	50.3	50.0
$l_c = (\gamma/\rho g)^{\frac{1}{2}}$ [cm]	0.273	0.226	0.226
$l_\nu = \rho\nu^2/\gamma$ [cm]	1.38×10^{-6}	2.79	1.15
$t_\nu = \nu^3\rho^2/\gamma^2$ [s]	1.91×10^{-10}	0.652	0.174

TABLE 1. The physical parameters for water at 20 °C and glycerol at 20 °C and 25 °C, quoted from Weast (1978). The first line contains the kinematic viscosity ν, the second the surface tension divided by density γ/ρ. The remaining three lines contain characteristic length- and timescales; g is the acceleration due to gravity.

dimensionless parameters controlling the problem are λ/r_0, l_ν/r_0, and the Weber number $\beta^2 = \rho r_0 V^2/\gamma$. Here $\lambda = V/f_p$ is the wavelength of the perturbation and l_ν the viscous length (29). Typical values for fluid parameters can be found in table 1. The jet experiments were done with water.

For the jet, the linearized problem of §2 now takes place in a semi-infinite geometry, where surface perturbations are prohibited to the left of the nozzle opening (Keller, Rubinow & Tu 1973; Leib & Goldstein 1986). However, for large Weber numbers (239 in the present experiment) the growth of unstable modes is just the same as the temporal growth of §2, translated into space via the jet velocity V. Also, the parabolic velocity profile of the nozzle opening has relaxed into a plug profile in the relevant region of the jet (Chaudhary & Maxworthy 1980), so we are assuming a constant profile right from the opening.

We follow the simulation up to the first singularity. The resulting profile is aligned with a picture of the experimental jet, to make the minima in front of the drop which is about to detach coincide. In figure 1 theoretical and experimental profiles are compared for $\lambda/r_0 = 14.57$. The case with the smallest perturbation is shown

(Chaudhary & Maxworthy 1980). Allowing for some blur of the photographs, the agreement in the shape of the drop about to form is quite nice. Note that the breakup is taking place in a very asymmetric fashion (with respect to the breakup point): on the right side the profile is quite steep forming a very much rounded drop; on the other side a flat neck formed, which will eventually coalesce into a smaller satellite drop.

An even more direct comparison is possible with an experiment investigating a dripping tap (Peregrine *et al.* 1990). As long as the drop is small, it will be suspended stably from the orifice. By slowly filling in more liquid, the drop goes through a series of stable states, until eventually gravity overcomes surface tension and the lower half of the drop falls. Subsequently, a thin neck forms and the lower part of the drop detaches. The stability of the drop hanging in equilibrium has been the subject of much study in itself (Michael & Williams 1976). The lengthscale controlling this problem is the capillary length

$$l_c = (\gamma/\rho g)^{\frac{1}{2}}. \tag{33}$$

For water, l_c and l_v, the viscous length, are separated by almost five orders of magnitude, see table 1. Hence there is a wide range of physical phenomena to explore between the onset of the linear instability and the breakup of the drop.

We will not repeat the stability analysis for our one-dimensional equations here, but concentrate on the breakup. The only dimensionless parameters in the problem are the ratios l_c/r_0 and l_v/r_0, where r_0 is the radius of the orifice. They were made to coincide with the experimental values, the working fluid being water.

There are some technical problems involved in simulating the moving boundary at the lower end of the drop. We avoid having to use a movable grid by mapping the problem on the unit interval, $z/l = x \in [0, 1]$, where l is the length of the drop which is calculated using

$$l(t) = \int_{t_0}^{t} v(1, s) \, \mathrm{d}s. \tag{34}$$

By definition, $v(1, s)$ is the velocity of the lower boundary. Care must also be taken to calculate the pressure at the endpoint where h_z becomes infinite. For the values $x \in [0.9, 1]$ we calculate p by interpolating $h(x)$ with an *even* fourth-order polynomial. Then all the singularities in the mean curvature cancel.

Figure 2 shows a series of profiles taken at constant time intervals of $0.4(r_0^3 \rho/\gamma)^{\frac{1}{2}}$. In the experiment, this would correspond to 6.6 ms. Given the very small timescale it would be very costly to let fluid drip as slowly as is possible in experiments. To still let initial oscillations die out, the viscosity is set to a very high value initially, and is then reduced to the value of water well before the first instability. Fluid is injected at the orifice with speed $0.02\gamma/(\rho r_0^{\frac{1}{2}})$. To the profiles at constant time intervals we add a snapshot of the drop as the width of the neck becomes $0.01r_0$. We also superimpose an experimental picture of the drop (Peregrine *et al.* 1990), taken at the point of breakup.

The very good agreement with simulations is especially impressive since this was not to be expected from a simple one-dimensional approximation. In particular in the lower half of the drop the assumption $h \ll l$ seems to fail, but one must remember that this part of the drop is almost static in a moving frame of reference. But the static limit of the equations is retained exactly in the approximation. Note that although the linear instability of the hanging drop is not investigated explicitly, it is also accurately described by the model. Namely, it determines the total volume of the drop (upper and lower half combined) and influences the point of breakoff.

Again, the breakoff occurs very asymmetrically, as was already observed in the jet decay. The asymmetry therefore does *not* come from the action of gravity. This is also
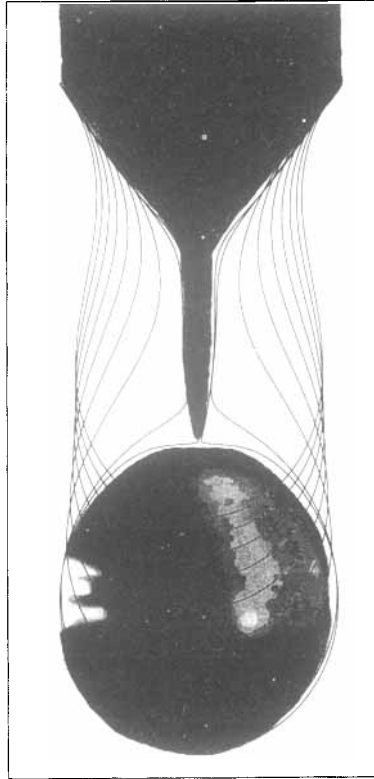
FIGURE 2. Simulation of a drop of water suspended from a circular orifice of radius $r_0 = 0.26$ cm. This gives parameter values $l_c/r_0 = 0.992$ and $l_\nu/r_0 = 4.89 \times 10^{-6}$, compare table 1. The time distance between profiles is $0.4(r_0^3 \rho / \gamma)^{\frac{1}{2}}$, starting from a point where the drop is already falling. We also superimpose a profile at the snap-off and the corresponding experimental picture from Peregrine *et al.* (1990). There is no adjustable parameter in the comparison. To enhance contrast, we erased the background in the original photograph.

confirmed by the estimate of Peregrine *et al.* (1990), who estimate that by the time the neck is formed, straining forces due to surface tension outweigh the straining forces due to gravity.

We conclude this section by reporting on a simulation of a fluid with significantly higher viscosity. With the radius of the orifice being 0.06 cm, we adjusted l_c/r_0 and l_ν/r_0 to match the parameter values for glycerol at 25 °C, as given in table 1. The viscosity of glycerol is about 1000 times higher than that of water, leading to a very different type of dynamics. Figure 3 shows the neck being pulled into a long and thin thread. Its length is 40 times the radius of the orifice at the point of rupture. Qualitatively, this is consistent with linear stability analysis: for high viscosity, the most unstable wavelength becomes large, see (32). On the other hand, the radius r_0 of the thread becomes very small, so (32) cannot account for its length in any quantitative way. The origin is clearly dynamical. The break occurs at the upper end of the thread in the simulation presented, but it may also happen close to the drop under slightly different conditions. Experiments with high-viscosity fluids in the same geometry are in progress (Shi & Nagel 1992).
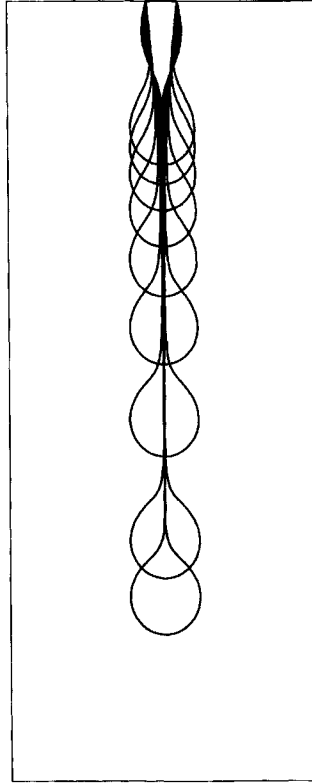
FIGURE 3. Same as figure 2, but with the fluid being glycerol at 25 °C and $r_0 = 0.0625$ cm. The parameters are now $l_c/r_0 = 3.61$ and $l_v/r_0 = 18.3$. Note the long neck, which is the trademark of high-viscosity fluids.

5. Nature of singularities

We now look closer at the point where the fluid neck is pinching off. As the radius goes to zero, pressure forces are expected to diverge, and the small amount of fluid left in the neck region is pressed out of it even faster. Therefore, as $h_{min} \to 0$, where h_{min} is the minimum radius, the velocity and higher derivatives of both h and v will probably become infinite at the point of rupture. This is the singularity or 'blow up' we want to investigate further.

Keller & Miksis (1983) present a very interesting scaling theory for the singularity in the non-viscous case. There are two important differences between our problem and theirs: their geometry is two-dimensional rather than three-dimensional-axisymmetric, and they study the time *after* the breakup.

The idea of their study may be described as follows: since h becomes very small near the singularity and v large, the pinch region is separated in scale from the boundaries. Therefore boundary conditions become irrelevant and the flow is determined by γ/ρ alone. If $\Delta t = t_s - t$ represents the time distance from the singularity, the only available lengthscale is the combination $(\gamma \Delta t^2/\rho)^{\frac{1}{3}}$. Hence, introducing

$$\bar{z} = (z - z_s)(\gamma \Delta t^2/\rho)^{-\frac{1}{3}}, \tag{35}$$

where z_s is the position of the pinch point, and

$$\bar{h} = h(\gamma \Delta t^2/\rho)^{-\frac{1}{3}}, \quad \bar{v} = v(\gamma/\rho \Delta t)^{-\frac{1}{3}}, \tag{36}$$

the problem can be written in terms of the similarity variables $\bar{z}$, $\bar{h}$, and $\bar{v}$ alone. Once
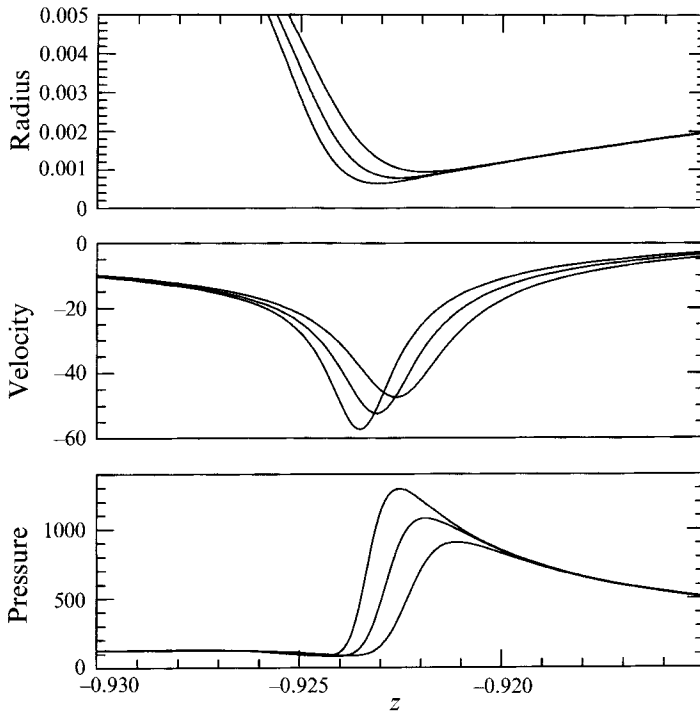
FIGURE 4. A close-up view of simultaneous radius, velocity, and pressure profiles close to pinch-off at three time distances Δt from the singularity: $\log_{10}(\Delta t) = -4.0$, -4.1, and -4.2, in units of γ/ρ and r_0. The viscosity is $\nu = 0.0037$. The pressure is higher on the right hand side of its peak, pushing fluid to the left. The minimum of the radius h moves with the fluid underneath it.

the similarity equation is solved, the resulting profile determines the evolution of the interface for all times up to the singularity. Note that $h \to 0$ and $v \to \infty$ as $\Delta t \to 0$ if $\bar{h}$ and $\bar{v}$ are assumed fixed, consistent with the original assumptions.

We will see, however, that this similarity argument does not carry through for the case of our equations, since the inviscid case appears to develop singularities even before $h_{min} \to 0$! For a consistent formulation up to the point of breakup we therefore need to add at least a small amount of viscosity. We are confident that the following conjecture, due to P. Constantin (private communication), is true. It indicates that with viscosity the singularity does not occur until h_{min} goes to zero.

CONJECTURE 1. *For $\nu > 0$ and $t \in [0, t_0]$ such that $h(t) \geqslant h_0 > 0$ the solutions of* (17), (18) *stay regular, i.e. h, v, and all their derivatives remain bounded in $[-l, l]$ for $t \in [0, t_0]$ with bounds depending only on ν and h_0.*

To investigate the problem further, we chose a cylinder of radius $r_0 = 0.01$ and length 2 as an initial condition. At its ends $z = \pm 1$ the radius is kept fixed and the velocity is set to zero. Given a slight initial disturbance in the velocity field, the cylinder collapses and forms a singularity after about $20(r_0^3 \rho/\gamma)^{\frac{1}{2}}$. The viscous length is $l_\nu = 1.4 \times 10^{-5}$.

The profile near the singularity comes out quite asymmetric, as observed before. This is also true if one starts from initial data almost symmetric around $z = 0$. Two almost linear pieces of different slope are joined smoothly by a round piece with a radius of curvature comparable to the minimum radius, cf. figure 4. Hence both terms in the pressure in (17) are of the same order of magnitude at the minimum, while the first term

dominates the linear regime away from the minimum. This means the pressure is higher on the shallow side of the minimum (right-hand side in figure 4), forcing fluid over to the steeper side (left-hand side in figure 4). As seen by comparing with the velocities in figure 4, the minimum is convected with the velocity of the fluid, so in the frame of reference of the minimum fluid is expelled on either side. At the same time this causes the left-hand side to get even steeper.

If there is no mechanism curbing this process, the slope will eventually get infinite. All our simulations, conducted with different initial radii and initial disturbances, show that for the inviscid equations exactly this happens and h_z goes to infinity *even before* h_{min} goes to zero. Note that l_ν is still less than 2% of the minimum height in figure 4, yet the inviscid equations already would have blown up at the times shown. If ν is finite, on the other hand, h_z turns out to be uniformly bounded by a constant which gets larger as ν decreases. Hence for finite, but arbitrarily small ν blow-up only occurs for $h_{min} \rightarrow 0$.

From the conjecture mentioned earlier we conclude that viscous solutions, up to some finite minimum radius h_0, can be well approximated by finite differences as long as the mesh is fine enough. Intuitively, one expects that the mesh size Δz should be at least of the order of h_0. We checked convergence near the singularity by conducting a series of runs with increasingly fine resolution. To save on computational effort, only the region around the singularity is highly resolved, the grid getting coarser by factors of 2 towards the outside. We plotted h_{min} and the maximum velocity v_{max} versus the time difference from the singularity on logarithmic scales, see figure 5. Lengths are shown in units of l_ν and times in units of the viscous timescale

$$t_\nu = \nu^3 \rho^2 / \gamma^2. \tag{37}$$

The plots agree up to the lengthscale of the coarser grid. We also monitored the highest derivatives in the problem, i.e. p_z and v_{zz}. The dashed vertical line indicates the point up to which they seemed well resolved. As can be seen in figure 5, problems with resolution occur when h_{min} is of the order of Δz, indicated by the horizontal line. Since the numerical viscosity NVT as introduced in §3 is approximately equal to $v\Delta z$, convergence for increasingly fine grids also demonstrates that it does not introduce artificial effects. For the finest resolution the numerical viscosity was less than a tenth of the physical viscosity in the centre of the grid. From all this we feel confident that the plot of our best-resolved run in figure 5 gives a faithful description of the original equations up to the point indicated.

Figure 5 indicates that v_{max} goes to infinity as the singularity $h_{min} \rightarrow 0$ is approached. All derivatives of the velocity as well as second or higher derivatives of the height are found to blow up even faster. This means that their asymptotic value increases faster than a negative power of Δz as we increase the resolution. The maximum value of h_z, however, approaches a constant as $h_{min} \rightarrow 0$. This is an important self-consistency property of our equations: The solutions never approach a situation where the surface parametrization is bound to break down.

There are some regions where $h_{min}(t)$ is close to a power law, but they never extend over more than two decades in lengthscales. In v_{max} there is even less of an indication of power-law behaviour. The decay of h_{min} is always faster than the $t^{\frac{2}{3}}$ power law predicted by (35), (36).

Considering also the profiles $h(z)$ and $v(z)$ directly, we conclude that (35), (36) are clearly not valid, even for $h_{min} \gg l_\nu$. The reason may be that $(h_z)_{max}$ goes to infinity long before h_{min} goes to zero, hence viscosity is important even on scales much larger than l_ν. The nature of the singularity of our inviscid equations probably is specific to the
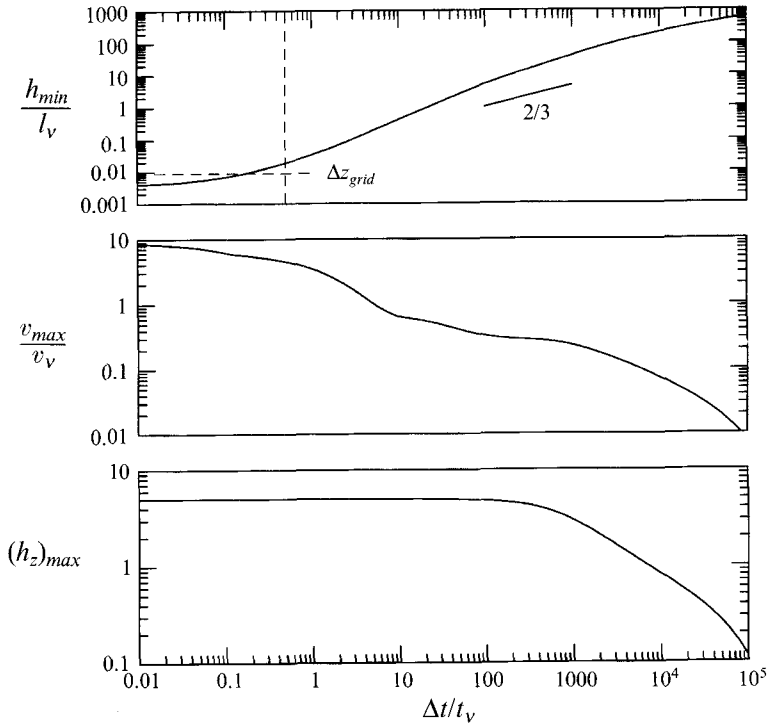
FIGURE 5. The minimum radius h_{min}, maximum (absolute) velocity v_{max} and the maximum (absolute) slope $(h_z)_{max}$ as functions of the time distance from singularity Δt, in units of the viscous scales l_ν, t_ν, and $v_\nu = l_\nu/t_\nu$. The axes are logarithmic. The dashed vertical line indicates the point where p_z is no longer fully resolved. This happens when h_{min} reaches the grid size. The $\frac{2}{3}$-slope would be predicted by a non-viscous similarity theory.

approximation. For example, it could be that the full Euler equations, instead of overturning, produce localized regions of high vorticity which our approximation cannot describe.

The system described so far is determined by the four parameters r_0, l, γ/ρ, and ν. If it has a solution $h(z, t)$ and $v(z, t)$, the system with parameters ar_0, al, $(a^3/b^2)\gamma/\rho$, $(a^2/b)\nu$ will have the scaled solution

$$h_{ab}(z, t) = ah(z/a, t/b),$$
$$v_{ab} = (a/b)v(z/a, t/b).$$

This is equivalent to saying that up to a rescaling of length and time the solution is determined by *two* dimensionless ratios, r_0/l and l_ν/l, say. By the argument presented at the beginning of this section, one expects the solution near the singularity to be independent of the dimensions of the initial cylinder. Hence *all* solutions, for $t \approx t_s$ and $z \approx z_s$, can be written in the universal form

$$\left. \begin{array}{l} h(z, t) = l_\nu h_s(\pm (z - z_s)/l_\nu, (t_s - t)/t_\nu), \\ v(z, t) = \pm (l_\nu/t_\nu) v_s(\pm (z - z_s)/l_\nu, (t_s - t)/t_\nu). \end{array} \right\} \tag{38}$$

The $\pm$ signs in (38) take care of the fact that the solutions may have different parity, with fluid flowing from left to right or vice versa.

We tested (38) by conducting simulations with different parameter values and calculating h_s and v_s from them. Namely, we increased r_0 by a factor of 10 and also
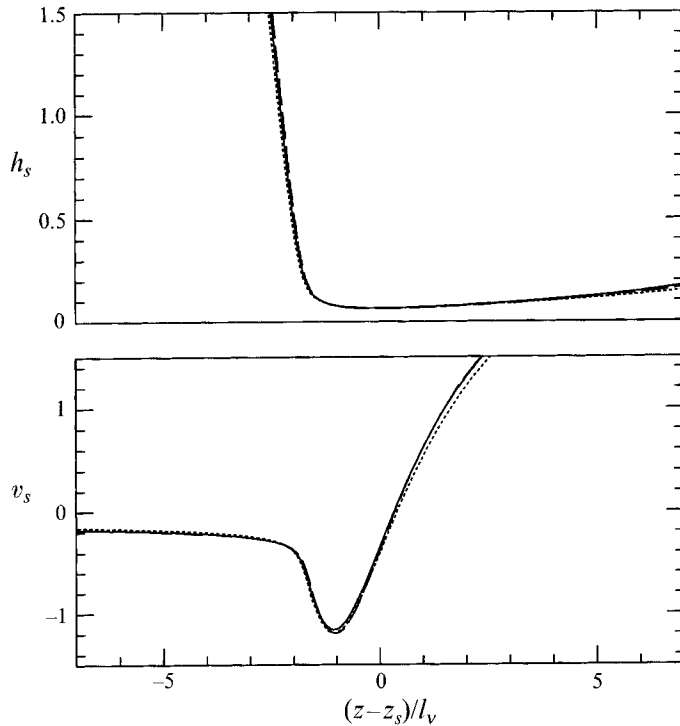
FIGURE 6. The reduced profiles h_s and v_s as calculated from different parameter values $(r_0, l, \gamma/\rho, \nu)$ via (38) at $(t_s - t)/t_\nu = 1.97$. The solid line represents $(0.01, 1, 1, 0.0037)$, the dotted line $(0.1, 1, 1, 0.0037)$, and the long-dashed line $(0.01, 1, 1, 0.0074)$. The point of touch-down is shifted to zero in each case, the units are the viscous scales. The dotted lines had to be flipped over ($-$signs in (38)) to correct for the difference in parity.

varied the viscosity. This causes the global behaviour of the solution to change dramatically, yet on length and time scales comparable with l_ν and t_ν or smaller (38) is obeyed beautifully. Figure 6 shows h_s and v_s as calculated from different runs, all at $(t_s - t)/t_\nu = 1.97$. Note that the reduced profiles still evolve in time, unlike the similarity solutions of (35), (36).

6. Discussion

The key to the success of the present inve̊ṡṫigation lies in the construction of appropriate model equations to study the motion of thin columns of fluid. First, our expansion method allows viscous body forces as well as viscous boundary conditions to be taken into account. This makes it distinct from methods where the average velocity over the cross-section is the dynamical variable, such as in the equations for shallow water waves (Peregrine 1972). Precisely due to the inclusion of boundary conditions, the viscous terms in our equations become purely dissipative.

Second, we take the exact curvature term (17) into account. The importance of those higher-order terms of the expansion for strong variations of h was noticed before (Johnson *et al.* 1991). Figure 2, for example, beautifully demonstrates how the model takes equilibrium shapes into account. Also, regions of high slope ($h_z \approx 10$) at the top of the drop are very well represented.

Apart from experimental test, though, we do not see how to give *a priori* estimates of the quality of approximation in the framework of our model alone. A possibility is

to study the next order in the expansion. Apart from an equation of motion for h, we now have *two* equations for the expansion coefficients of the velocity field, $v_0(z, t)$ and $v_2(z, t)$. Those equations, although readily written down, are considerably more complicated than (17), (18) and require new numerical methods. Therefore, we consider it a study all of its own which should be investigated separately.

Most importantly, our equations remain self-consistent right up to the point of rupture $h_{min} \to 0$. This means that no other singularity occurs before that point. This is supported by our simulations over a wide range of viscosities and by preliminary mathematical analysis (P. Constantin, private communication). Specifically, there is no overturning of the profile. The full equations of motion certainly would not form singularities even in the case of overturning, but there does not seem to be experimental evidence for this to occur before breakup. (This excludes initial or boundary conditions with strong transversal velocity gradients, which 'force' the flow to overturn, but which are not realizable in our equations in the first place.) Hence we see no reason to doubt the applicability of our model even for small viscosities such as in water.

However, the inviscid version of our equations clearly is at odds with experimental evidence, showing overturning on experimentally accessible timescales. This reflects the singular nature of the limit $\nu \to 0$. We hope this will shed some light on the nature of this limit in the Navier–Stokes equation and its relation to the Euler equation.

We plan to develop a code with an adaptable grid, which moves with the position of the minimum and introduces new grid points when needed. This code is expected to be much more effective and to allow us to reach considerably higher resolution. We hope this will allow us to explore the asymptotic regime even more carefully.

Another expected benefit of the new code is to be able to go *beyond* the first singularity by introducing a new grid point at the pinch. The equations will then be integrated from there with new boundary conditions. This will allow us to investigate a new range of phenomena, like formation of satellite drops, recoiling, etc.

In conclusion, we have developed a one-dimensional equation for an axisymmetric thread of fluid. Computed profiles coincide nicely with experiments. The inviscid equations are inconsistent, leading to singularities even before the breakup into drops. All solutions with $\nu > 0$ are described by the universal scaling functions h_s, v_s sufficiently close to the singularity.

REFERENCES

BECKER, E., HILLER, W. J. & KOWALEWSKI, T. A. 1991 Experimental and theoretical investigation of large-amplitude oscillations of liquid droplets. *J. Fluid Mech.* **231**, 189–210.

BOGY, D. B. 1979 Drop formation in a circular liquid jet. *A. Rev. Fluid Mech.* **11**, 207–228.

CARMO, M. P. DO 1976 *Differential Geometry of Curves and Surfaces*. Prentice-Hall.

CHANDRASEKHAR, S. 1961 *Hydrodynamic and Hydromagnetic Stability*, Chap. 12. Clarendon.

CHAUDHARY, K. C. & MAXWORTHY, T. 1980 The nonlinear capillary instability of a liquid jet. Part 2. Experiments on jet behaviour before droplet formation. *J. Fluid Mech.* **96**, 275–286.

CHAUDHARY, K. C. & REDEKOPP, L. G. 1980 The nonlinear instability of a liquid jet. Part 1. Theory. *J. Fluid Mech.* **96**, 257–274.

CONSTANTIN, P., DUPONT, T. F., GOLDSTEIN, R. E., KADANOFF, L. P., SHELLEY, M. & ZHOU, S. M. 1993 Droplet breakup in a model of the Hele–Shaw cell. *Phys. Rev.* E **47**, 4169–4181.

CRAM, L. E. 1984 A numerical model of droplet formation. In *Computational Techniques and Applications: CTAC-83* (ed. J. Noye & C. Fletcher). Elsevier.

JOHNSON, M., KAMM, R. D., HO, L. W., SHAPIRO, A. & PEDLEY, T. J. 1991 The nonlinear growth of surface-tension-driven instabilities of a thin annular film. *J. Fluid Mech.* **233**, 141–156.

KELLER, J. B. & MIKSIS, M. J. 1983 Surface tension driven flows. *SIAM J. Appl. Maths* **43**, 268–277.

KELLER, J. B., RUBINOW, S. I. & TU, Y. O. 1973 Spatial instability of a jet. *Phys. Fluids* **16**, 2052–2055.

LANDAU, L. D. & LIFSHITZ, E. M. 1984 *Fluid Mechanics*. Pergamon.

LEE, H. C. 1974 Drop formation in a liquid jet. *IBM J. Res. Dev.* **18**, 364–369.

LEIB, S. J. & GOLDSTEIN, M. E. 1986 The generation of capillary instabilities on a liquid jet. *J. Fluid Mech.* **168**, 479–500.

MAJDA, A. 1986 Vorticity and the mathematical theory of incompressible fluid flow. *Commun. Pure Appl. Maths.* **39**, S187–S220.

MESEGUER, J. 1983 The breaking of axisymmetric slender liquid bridges. *J. Fluid Mech.* **130**, 123–151.

MICHAEL, D. H. & WILLIAMS, P. G. 1976 The equilibrium and stability of axisymmetric pendant drops. *Proc. R. Soc. Lond.* A **351**, 117–127.

PEREGRINE, D. H. 1972 Equations for water waves and the approximation behind them. In *Waves on Beaches* (ed. R. E. Meyer). Academic.

PEREGRINE, D. H., SHOKER, G. & SYMON, A. 1990 The bifurcation of liquid bridges. *J. Fluid Mech.* **212**, 25–39.

RAYLEIGH, LORD 1878 On the instability of jets. *Proc. Lond. Math. Soc.* **4**, 10.

SHI, X. D. & NAGEL, S. R. 1992 Droplet formation (unpublished).

SMOLLER, J. 1983 *Shock Waves and Reaction-Diffusion Equations*, Chap. 15. Springer.

WEAST, R. C. (ed.) 1978 *Handbook of Chemistry and Physics*. CRC Press.